Investigation of Spillover Mechanism in Palladium Decorated Hydrogen Exfoliated Functionalized Graphene

ARTICLE *in* THE JOURNAL OF PHYSICAL CHEMISTRY C · JULY 2011

Impact Factor: 4.77 · DOI: 10.1021/jp202797q

4 AUTHORS, INCLUDING:

B P Vinayan
Helmholtz-Institut Ulm
32 PUBLICATIONS **505** CITATIONS
SEE PROFILE

Rupali Nagar
Symbiosis Institute of Technology
21 PUBLICATIONS **444** CITATIONS
SEE PROFILE

THE JOURNAL OF PHYSICAL CHEMISTRY C

ARTICLE

pubs.acs.org/JPCC

Investigation of Spillover Mechanism in Palladium Decorated Hydrogen Exfoliated Functionalized Graphene

Vinayan Bhagavathi Parambhath,[†,‡] Rupali Nagar,[†] K. Sethupathi,[‡] and S. Ramaprabhu[†,*]

[†]Alternative Energy and Nanotechnology Laboratory (AENL), [1]Nano Functional Materials Technology Centre (NFMTC)

[‡]Low Temperature Physics Laboratory, Department of Physics, Indian Institute of Technology Madras, Chennai, Tamil Nadu, 600036, India

Supporting Information

ABSTRACT: Porous activated carbon or nanostructured carbon materials have a promising future as hydrogen storage media. The hydrogen storage capacity of nanostructured carbon materials can be further enhanced by spillover of atomic hydrogen from a supported catalyst. In the present work, both of these factors have been put to test to study the hydrogen storage capacity of palladium (Pd) nanoparticles dispersed over the surface of functionalized hydrogen-exfoliated-graphene (Pd/*f*-HEG). The high-pressure hydrogen storage measurements of HEG and Pd/*f*-HEG show a hydrogen storage capacity of 0.5 and 1.76 wt % respectively at 25 °C and 2 MPa pressure. Functionalization of graphene facilitates uniform dispersion of Pd nanoparticles, which result in an increased hydrogen storage capacity of graphene by 69%. Heats of adsorption have been calculated for HEG and Pd/*f*-HEG that are consistent with the theoretical calculations from literature and provide an experimental evidence for the spillover effect.

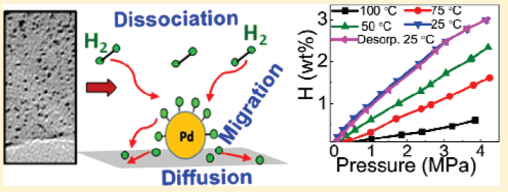

INTRODUCTION

Hydrogen has emerged as one of the viable options catering to the energy requirements of the world in near future. Being a renewable energy carrier, it relaxes concerns related to depleting fuels. In addition, it has high energy density by mass and is environmentally benign due to its zero-emission properties. In 2003, the Department of Energy convened a task force that identified storage of hydrogen as the most difficult challenge.[1] The safe storage of hydrogen, low hydrogen-storage capacities by materials until date, and cost effectiveness of a hydrogen economy are the factors that have prevented the replacement of conventional sources of energy by hydrogen-based storage media.

For practical applications, hydrogen storage demands high gravimetric and volumetric densities, fast reaction kinetics, a low H_2 sorption temperature, good reversibility, and low cost. Physical storage of hydrogen by liquefaction or pressurization requires high energy input and safety risks are involved. Chemically stored hydrogen in materials is a safe and efficient means of storing hydrogen. Presently, in the various hydrogen storage methods, nanostructured carbon materials have been the popular choice of materials due to their lightweight, high surface areas and relative chemical stabilities.[2] The carbon materials that have been focused are graphite, carbon nanofibers, activated carbon, and carbon nanotubes (CNTs). The hydrogen uptake capacity of CNTs is usually less than 1 wt %.[3] At low temperatures of around ~80 K, the reported hydrogen uptake capacity of carbon materials prepared by different methods varies in a wide range and evidently remains higher than those at room temperature. A rich literature exists on the study of hydrogen storage by carbon-based materials. For instance, Ma et al. reported that a single layer of graphene could store 0.4 wt % hydrogen at 100 kPa pressure and cryogenic temperature.[4] However, at room temperature the adsorption capacity decreased to 0.2 wt % for 6 MPa pressure. In another study, Choi et al. showed that KOH activated carbon could store about 0.75 wt % hydrogen at 10 MPa.[5] By combining the techniques of composition doping and textural adjustment, Jiang et al. demonstrated that nitrogen containing carbon spheres could store 2.21 wt % hydrogen at room temperature and 8 MPa pressures.[6] It was further shown by Orimo et al. that nanostructural graphite can amass about 7.4 wt % hydrogen during mechanical milling by chemisorption.[7] Despite numerous studies, a technologically sound and economically viable material has not been suggested that has good hydrogen storage properties at ambient or near ambient temperatures and pressures. This has led to the onset of consolidated efforts in combining the merits of individual materials and studying the newly formed composites.

There are broadly two ways to enhance the uptake capacity by any adsorbent material namely, increasing its surface area or its affinity toward the adsorbent species. An adsorbent with high surface area and pore volume has a large number of adsorption sites and is anticipated to be an excellent candidate as an adsorbent. In this context, graphene, a one atom thick sheet of hexagonal carbon atoms, has attracted a great deal of interest due to its extremely large surface area and unique material properties such as high mobility of charge carriers, high thermal conductivity, and high mechanical strength.[8,9] However, synthesis of single

Received: March 25, 2011
Revised: June 16, 2011
Published: June 23, 2011

sheets of graphite in large quantities is extremely difficult. Thus, recent reports have indicated the use of graphene nanoplatelets or layered graphene sheets.[10,11] To increase the affinity or selectivity for a particular adsorbent, chemically favorable species can be utilized. Recently, it was reported that hydrogen storage at room temperature can be improved by a phenomenon known as *spillover effect* initiated by metal nanoparticles decorated over the adsorbate surface.[12,13] Hydrogen spillover is defined as the dissociative chemisorption of hydrogen molecules on metal nanoparticles in the form of atomic hydrogen and subsequent migration of these hydrogen atoms onto adjacent surfaces of the adsorbate via surface diffusion.[12,13] The contact between the metal nanoparticles and supporting adsorbate material plays a major role in spillover mechanisms. Doping or chemically modifying the supporting material can significantly affect the spillover of H_2 molecules.[14] However, the issue of structural stability and poor reversibility in transition metal dispersion has been a major concern because the transition metal atoms tend to aggregate easily because of the strong metal cohesion forces. To avoid agglomeration of transition metal nanoparticles, it was suggested to increase the binding energy between metal and adsorbate materials by introducing structural or chemical defects.[15] Theoretical studies have aided in this context considerably. For instance, first-principle studies by Banerjee et al. show that transition metal atoms on Mg surface influence the hydrogen dissociation or hydrogen diffusion barriers.[16,17] A proper choice of substitutional metal atoms may therefore enhance the hydrogen storage capacity.

In this article, we explore the possibility of combining the merits of higher surface area of graphene sheets along with use of Pd metal nanoparticles for hydrogen storage applications. A novel and easy technique for rapid and large-scale synthesis of exfoliated graphene sheets was recently reported by us that resulted in high-quality graphene sheets.[18] An optimum dispersion of palladium nanoparticles over the surface of hydrogen-exfoliated graphene was obtained by modified ethylene glycol reduction method. High-pressure hydrogen adsorption−desorption properties of hydrogen-exfoliated graphene and Pd-decorated hydrogen-exfoliated graphene were studied.

EXPERIMENTAL METHODS

Graphite (99.99% SP-1, Bay carbon) with average particle size of 45 μm, sodium nitrate ($NaNO_3$, 99.5%), potassium permanganate ($KMnO_4$, 99.5%), and concentrated sulphuric acid (98%) (Rankem Chemicals, India) were used. Palladium(II) chloride (99%), and ethylene glycol (99%) were purchased from Sigma−Aldrich. Hydrogen peroxide (H_2O_2, 30%) was procured from S D Fine-Chem. Ltd., India.

Graphene was synthesized by exfoliation of graphitic oxide. Initially, graphitic oxide (GO) was prepared from purified natural graphite using Hummers' method.[19] In this method, 2 g of graphite was added to 46 mL of conc. H_2SO_4 under continuous stirring in an ice bath. One gram $NaNO_3$ and 6 g $KMnO_4$ were added gradually and successively. The suspension was removed from the ice bath and was allowed to come to room temperature. Next, 92 mL of water was added to the above mixture. After 15 min, the above mixture was diluted by adding 280 mL of warm water. Following this, 3% H_2O_2 was added until the solution turned bright yellow. The suspension was filtered and the filter cake was repeatedly washed with warm water. The residue was diluted using water and the resulting suspension was centrifuged. The final product was dried under vacuum and stored in vacuum desiccators until further use.

Exfoliation of GO was carried out as follows. The sample was taken in a quartz boat and placed inside a tubular furnace. The furnace was sealed at both the ends with end couplings having provision for gas flow. The furnace was flushed with Argon (99.99%) for 15 min. The temperature of the furnace was then raised to ∼250 °C. Highly pure H_2 gas (99.99%) was allowed at this temperature. Exfoliation occurred within one minute, which was easily visible. For dispersing metal nanoparticles over graphene, the as-prepared hydrogen-exfoliated graphene (HEG) was functionalized by stirring it continuously in a solution of concentrated sulfuric acid and concentrated nitric acid (3:1) for 3 h. The functionalized hydrogen-exfoliated graphene was labeled as *f*-HEG.

To prepare the palladium-decorated graphene by modified polyol method, about 300 mg of *f*-HEG was dispersed in 300 mL of a mixture of ethylene glycol (EG) and water by ultrasonication for 1 h and followed by stirring for 12 h. Further, the required amount of 1% aqueous solution of $PdCl_2$ (6 mg of Pd/mL of deionized (DI) water) was added to the solution dropwise under mechanically stirred conditions for 24 h. The pH of the entire solution was adjusted to 11 by adding NaOH (2.5 M) and the solution was refluxed at 110 °C for 7 h to ensure that the entire Pd was completely reduced. The water to EG ratio was controlled 1:3 throughout the reaction. In this reaction, ethylene glycol acts as a reducing, stabilizing, and dispersing agent. Finally, the suspension was filtered and the solid washed with DI water repeatedly until neutral and dried in vacuum oven at 50 °C. The samples synthesized by modified polyol method were labeled as Pd/*f*-HEG.

Powder X-ray diffraction (XRD) studies were carried out using a PANalytical X'Pert Pro X-ray diffractometer with nickel-filtered Cu Kα radiation as the X-ray source. The sample was scanned in steps of 0.016° in the 2θ range 5−90°, where 2θ is the Bragg angle. Functional group identification was done using a PerkinElmer FTIR spectrometer. The vibrational characteristics of the samples were analyzed via Raman spectroscopy using a 532 nm laser (Witec Alpha 300) as the excitation source in the range 100−3000 cm^{-1}. The morphology of the samples was characterized by field emission scanning electron microscopy (SEM, FEI QUANTA 400F) and transmission electron microscope (TEM, JEOL JEM- 2010F). Brunauer−Emmett−Teller (BET) surface area analysis was determined by recording nitrogen adsorption/desorption isotherms at 77 K using a static volumetric technique with a Micromeritics ASAP V3.01 G 2020 instrument.

Hydrogen adsorption studies were carried out for the HEG and Pd/*f*-HEG in the pressure range 0.1−4 MPa and in the temperature range 25−100 °C using a high-pressure Sieverts' apparatus. The schematic representation of the setup is given in Figure 1. The unit was calibrated with high-purity hydrogen (99.99%) at various initial pressures. At various pressures and temperatures, the volume of gas contained in the empty sample cell was precisely measured. At high pressures, the ideal gas law was corrected using van der Waals equation for the volume of gas molecules and molecular interactions. A number of empty tests were performed, which confirmed that the system was leak free. Each time, over 250 mg of sample was loaded in the sample cell. The samples were activated by vacuum heat treatment before exposing to hydrogen to remove the impurities such as the adsorbed water and oxide layers. In each activation process, the

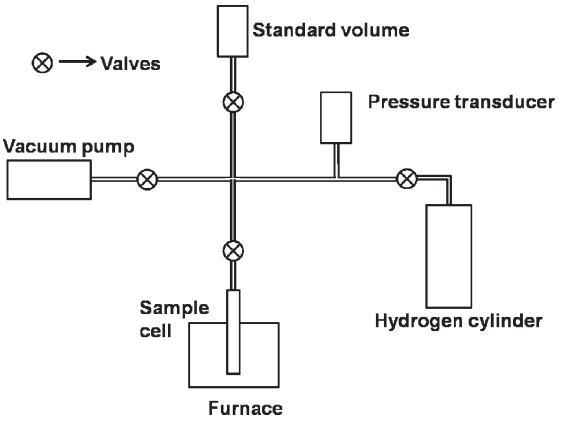

Figure 1. Schematic of high-pressure Sieverts' apparatus for hydrogen adsorption.

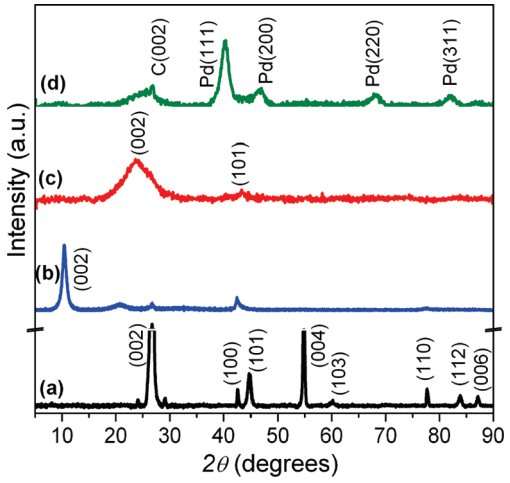

Figure 2. XRD pattern of (a) graphite, (b) GO, (c) HEG, and (d) Pd/*f*-HEG.

sample was evacuated to a vacuum of 10^{-6} Torr and heated at 200 °C for 3 h. It was then cooled to 100 °C and hydrogen was allowed to interact with the sample. The sample was subsequently cooled to 75 °C, 50 °C, and room temperature. The pressure−composition relationships were obtained by calculating the hydrogen storage capacity in wt % from the pressure drop during the hydrogen adsorption at constant temperature. After each cycle, the sample was degassed for 3 h at 200 °C under a vacuum of 10^{-6} Torr. During the experiment, the room temperature was maintained at 25 ± 1 °C.

RESULTS AND DISCUSSION

Structural and Surface Analysis. Figure 2 presents the powder X-ray diffractograms of (a) graphite (Gr), (b) GO, (c) HEG, and (d) Pd/*f*-HEG, respectively. An intense crystalline peak occurs at a 2θ value of 26.73°, which is the characteristic peak of the (002) plane in hexagonal graphite with a *d*-spacing of 0.34 nm. The presence of other peaks has been indexed in the figure. Upon oxidation, the peak shifts to 10.54° as seen in part b of Figure 2, which corresponds to the (002) plane of graphite oxide. An increase in the interlayer spacing to 0.84 nm has been observed. This increase in *d*-spacing is due to the intercalation

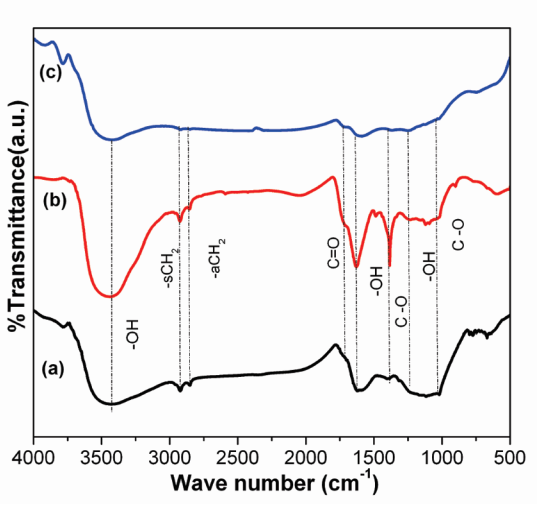

Figure 3. FTIR spectra of (a) HEG, (b) *f*-HEG, and (c) Pd/*f*-HEG.

of −OH containing functional groups in between the graphene layers. Four more peaks, though of lesser intensity, are observed in the case of GO. The peaks appear at 2θ values of 20.75°, 26.73°, 42.59°, and 77.6°, which indicate the presence of graphite phase. This may be due to incomplete oxidation of graphite.[20] After exfoliation of GO with hydrogen at ∼200 °C, the 10.54° peak disappears and a broad peak ranging from 14° to 30° appears (part c of Figure 2). This broad peak is suggestive of a loss of the long-range order in the stacked layers of graphene. The interlayer spacing decreases to 0.37 nm, which suggests the removal of oxygen and water from the layers during exfoliation. The interlayer spacing of exfoliated graphene is higher than the starting graphite powder (0.34 nm) suggesting loosening of graphene layers along the *c* axis. The fingerprint peaks of palladium appear along with broad peak of graphene as shown in part d of Figure 2, respectively. The broad peaks of Pd(111) clearly indicate the nanostructured nature of the particles. The particle size of Pd nanoparticles were estimated to be ∼6.6 nm using Scherrer's formula.

Parts a, b, and c of Figure 3 show the Fourier transform infrared spectroscopy (FTIR) spectra of HEG, *f*-HEG, and Pd/*f*-HEG, respectively. Part b of Figure 3 clearly shows the increase in the peak intensities of different functional groups after the process of functionalization. A strong and broad peak can be seen around 3436 and 1630 cm^{-1} in parts a−c of Figure 3 that corresponds to the stretching mode of the O−H group.[21] The peaks at 2925 and 2855 cm^{-1} are due to asymmetric and symmetric stretching of $-CH_2$.[22] The peaks at 1720, 1380, and 1228 cm^{-1} are attributed to C═O, C−O, and −OH of the −COOH groups, respectively. In part c of Figure 3, the peak intensities of functional groups have reduced, which indicates the attachment of Pd nanoparticles onto the functional groups. The Pd nanoparticles attach to graphene support via the oxygen containing functional groups. This has also been confirmed by X-ray photoelectron spectroscopy (Figure S1 of the Supporting Information).

Figure 4 represents the Raman spectra of (a) graphite, (b) GO, (c) HEG, (d) *f*-HEG, and (e) Pd/*f*-HEG, respectively. The absence of D band in graphite shows that initial graphite used was defect free. Analogous to the optically allowed E_{2g} phonons at the brillouin zone center, a highly intense G band, occurs at

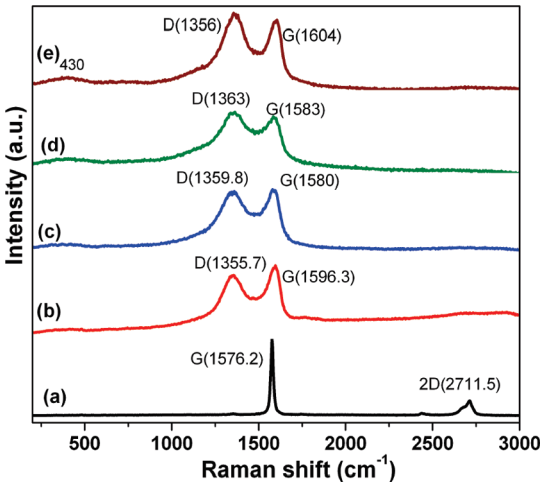

Figure 4. Raman spectra of (a) graphite, (b) GO, (c) HEG, (d) *f*-HEG, and (e) Pd/*f*-HEG.

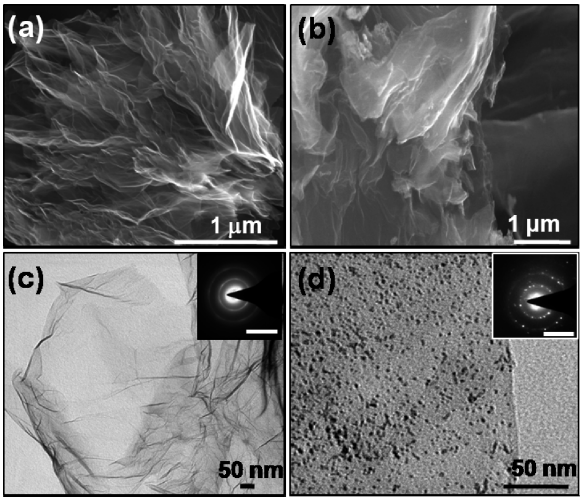

Figure 5. FESEM image of (a) HEG and (b) Pd/*f*-HEG. TEM image of (c) HEG and (d) Pd/*f*-HEG [insert image of parts c and d of Figure 5 show the diffraction pattern of HEG and Pd/*f*-HEG, respectively. The scale bars correspond to 5 nm^{-1}].

~1576.2 cm^{-1}.[23] The G band of GO is present at 1596.3 cm^{-1}, but for HEG which shifts back to 1580 cm^{-1}, close to the value of pristine graphite, indicating the reduction of GO during hydrogen exfoliation. In addition, a broadening of G band was observed in GO and HEG and is attributed to an increase in the disorder of the samples as also confirmed by the broadening of XRD peaks discussed above. The chemical treatments done to obtain GO and its exfoliation to obtain graphene induce defects in the graphitic structure. As a result, a broad D band with an intensity comparable to that of the G band is observed in the cases of GO and HEG samples. Quite often, the ratio between the intensities of the D and G bands is used to predict the presence of defects in the samples. The ratio of peak intensities of D and G bands (I_D/I_G) for GO, HEG, and *f*-HEG have been estimated to be around 0.92, 0.98, and 1.01, respectively. The functionalization increases the defects on the graphene surface, which enhance the intensity of D band in the Raman spectrum of *f*-HEG.[24] In the case of Pd/*f*-HEG (part e of Figure 4), similar peaks appear but at shifted

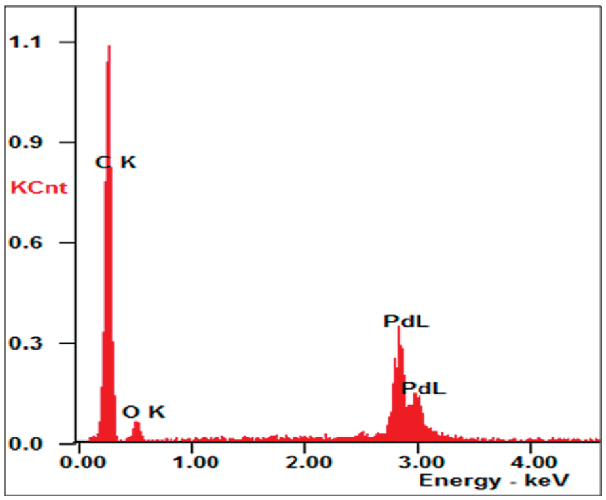

Figure 6. Energy dispersive X-ray analysis of Pd/*f*-HEG.

positions, which is primarily due to the metal−carbon interactions. The spectrum shows an additional peak at ~430 cm^{-1} due to the presence of palladium.

The BET surface area of the exfoliated graphene has been found to be 470 $m^2\ g^{-1}$ by studying the nitrogen adsorption−desorption isotherms. The measurements confirm the higher surface area of the adsorbate being used. Figure 5 shows the SEM images of (a) HEG, (b) Pd/*f*-HEG. Hydrogen exfoliation is a quick, easy, and efficient process for destacking the graphene sheets as evident from the multitude of the layers seen in part a of Figure 5. It is noteworthy that there are signs of graphene sheets stacking back together to a small extent in Pd/*f*-HEG samples as shown in part b of Figure 5. We believe that this slight restacking of the graphene sheets may occur during the functionalization of HEG. The functionalization of HEG facilitates an efficient binding of Pd nanoparticles to the carbon support.[25] The Pd nanoparticle dispersion on the graphene sheets was observed to be fairly uniform from the transmission electron micrographs as depicted in part d of Figure 5 for Pd/*f*-HEG. For comparison, the TEM image of HEG is shown in part c of Figure 5. The inserts in parts c and d of Figure 5 present the electron diffraction patterns (DPs) for HEG and Pd/*f*-HEG respectively acquired during TEM investigation. In the case of HEG, brighter arcs are visible (part c of Figure 5), which may be attributed to the presence of large size crystallites of graphene sheets (4−5 layers stacked together along (002) plane as observed from XRD analysis) along with fainter rings that indicate their amorphous nature. In case of Pd/*f*-HEG, the presence of spots in the DPs indicates that the samples have a polycrystalline nature and have been indexed as the Pd(111) and Pd(200) planes. Figure 6 shows the energy dispersive X-ray (EDX) analysis of Pd/*f*-HEG, indicating a 20 wt % Pd metal loading on HEG.

Hydrogen Storage Studies of HEG and Pd/*f*-HEG. Figures 7 and 8 show the pressure−composition isotherm of HEG and Pd/*f*-HEG in the temperature range 25−100 °C and the pressure 1−4 MPa, respectively. The hydrogen uptake capacity at all pressures decreases with increase in temperature, whereas the gradual increase of adsorption with hydrogen pressure is quite similar to the Langmuir isotherms.[26] The isotherms for HEG and Pd/*f*-HEG were found to be highly reversible at room temperature as can be seen from the desorption isotherms. The hydrogen

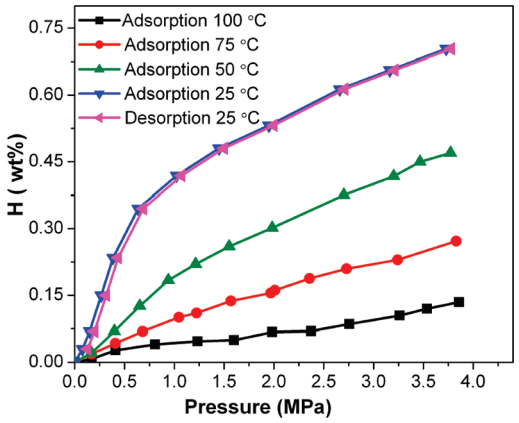

Figure 7. Hydrogen adsorption−desorption isotherms of HEG sample in the temperature range of 25−100 °C and pressures up to 4 MPa.

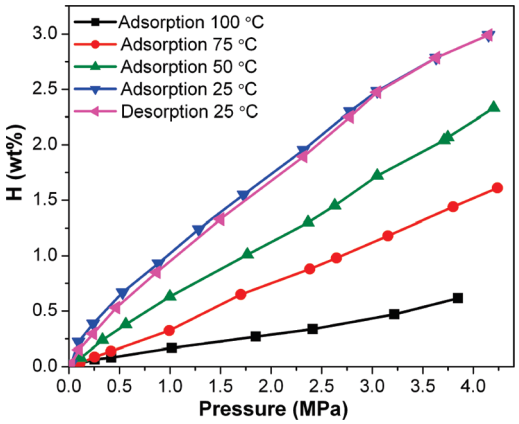

Figure 8. Hydrogen adsorption−desorption isotherms of Pd/*f*-HEG sample in the temperature range of 25−100 °C and pressures up to 4 MPa.

uptake capacity of HEG and Pd/*f*-HEG at 25 °C and 2 MPa pressure were observed to be 0.5 and 1.76 wt %, respectively. The isosteric heat of adsorption (Q_{st}) of H_2 has been calculated from the temperature dependence of H_2 adsorption isotherms by using the Clausius−Clapeyron equation as:[27]

$$Q_{st} = -R\left[\frac{\partial \ln P}{\partial(1/T)}\right]_n = -R\alpha \qquad (1)$$

where Q_{st} is the isosteric heat of adsorption, R is ideal gas constant, α is the slope of ln P versus $1/T$ at constant hydrogen adsorption amount n. The overall heats of adsorption of H_2 on the HEG and Pd/*f*-HEG samples were calculated from the isotherms at 25, 50, 75, and 100 °C by using the eq 1. It is to be noted that the calculated value of Q_{st} varies with the amount of hydrogen stored by the specimen. Therefore, the isosteric heats of adsorption for the case of HEG and Pd/*f*-HEG have been compared for 0.2 to 0.7 wt % of the hydrogen stored in the samples. The estimated value of Q_{st} for HEG was found to be 6−9 kJ mol^{-1} in the temperature range 25−100 °C, whereas for Pd/*f*-HEG it was found to be 8.87−12.5 kJ mol^{-1}. In case of Pd/*f*-HEG, the Q_{st} value of 7 kJ mol^{-1} has been estimated for 2.5 wt %. The isosteric heat of adsorption of HEG is higher than that of recently reported values for graphene and carbon nanotubes.[2,28] It is, however, in good agreement with recent theoretical studies, which predict an approximate binding energy on graphene to be 5.9 kJ mol^{-1}.[29] This suggests a strong interaction between adsorbed hydrogen and the surface of graphene. The values of Q_{st} have been tabulated in Table I. In a study reported by Bhatia et al. on adsorptive storage, optimum thermodynamic conditions for hydrogen adsorption have been estimated by employing Langmuir equation.[30] An adsorptive enthalpy of 15.1 kJ mol^{-1} has been found to be optimum for operation conditions of 0.15−3 MPa pressure and 300 K temperature. Our results show that Pd/*f*-HEG meets the criterion for optimum enthalpy for 2 MPa pressure and ambient temperature. Also, the desorption curve in Figure 8 exhibits complete reversibility corroborating the theoretical results reported by Bhatia et al. The increased isosteric heat of adsorption in case of Pd/*f*-HEG with respect to that of HEG suggests that the dispersed Pd nanoparticles over the surface of graphene induce some chemisorption of hydrogen along with physisorption, which enhances the interaction of H_2 with Pd/*f*-HEG. The hydrogen storage capacity of HEG and Pd/*f*-HEG is higher than that of the previous results on Pd-decorated high surface area carbons and carbon nanotubes.[31,32] Previous studies on Pd loaded carbon nanotubes have shown a hydrogen storage capacity of 0.66 wt % at room temperature and 2 MPa pressures.[32] Srinivas et al. have shown that extrapolation of the isotherms of graphene nanosheets to 10 MPa predicts hydrogen adsorption capacity of 0.72 wt % at 25 °C.[28] On extrapolation of isotherms to 10 MPa at 25 °C for HEG and Pd/*f*-HEG, we find hydrogen adsorption capacities of 1.2 and 5.3 wt %, respectively. This amounts to an enhancement of over 300%.

Table I. Isosteric Heat of Adsorption (Q_{st}) for Different Hydrogen Adsorption Amounts *n*

	Q_{st} (kJ mol^{-1})	
n wt% of hydrogen	HEG	Pd/*f*-HEG
0.2	9.15	12.5
0.3	8	11.52
0.6	6.78	10.44
0.7	6.03	8.87

Theoretical calculations show that decoration with transition metals on defected graphene can enhance the hydrogen storage capacity via spillover mechanism. In Pd/*f*-HEG the hydrogen molecules undergo dissociative chemisorptions on the surface Pd nanoparticles followed by migration of hydrogen atoms onto the surface of the metal particles and subsequent diffusion away from the receptor site and which has been shown by the schematic diagram in Figure 9. There are mainly three factors affecting the hydrogen storage capacity by spillover. One is the hydrogen dissociation source. In Pd/*f*-HEG, the Pd nanoparticles act as hydrogen dissociation sources and their effect on hydrogen storage has been intensively studied.[33,34] The second factor is the contact between the dissociation source and receptor. Because of the existence of physical and energy barriers for spillover of hydrogen atoms from the source to the receptor, an intimate contact between them could facilitate the spillover and thus result in enhancement of hydrogen storage capacity. In our case, the chemical modification of HEG via functionalization helps to make a strong contact between Pd nanoparticle and graphene surface. The third factor is the nature of the spillover hydrogen receptor. It has become clear that the enhanced

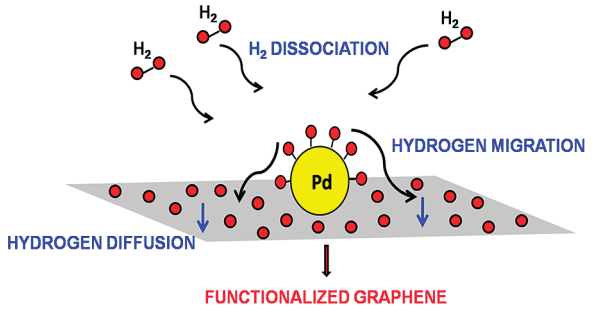

Figure 9. Schematic diagram of the spillover mechanism in Pd/*f*-HEG.

hydrogen storage capacity could be achieved on a receptor with a high surface area, which provides more adsorption sites for hydrogen atoms. Our results are the first experimental evidence to theoretical calculations, which show that transition metals on defected graphene can enhance the hydrogen storage capacity via spillover mechanism.[15,35−37] In Pd/*f*-HEG (section 2 of the Supporting Information) the hydrogen molecules undergo dissociative chemisorptions on the surface of Pd nanoparticles followed by migration of hydrogen atoms onto the surface of the metal particles and subsequent diffusion away from the receptor site.[38]

The enhanced hydrogen storage capacity observed for Pd/*f*-HEG found in the present work can be qualitatively accounted for by considering the contribution of palladium particles on the hydrogen storage. To get the exact value of enhanced hydrogen storage capacity of HEG, it is necessary to deduct the amount of hydrogen adsorbed by the Pd particles forming stable hydrides under the experimental conditions employed in the present work. For this, we have experimentally determined the amount of hydrogen stored in the pure Pd and then by assuming that the hydrogen uptake contribution of Pd particles is independent of the presence of carbon, the amount of hydrogen in the carbon phase was estimated. For Pd, the bulk storage capacity of hydrogen corresponds to a hydrogen-to-metal ratio of 0.7. The amount of Pd present in the sample has been found to be 20 wt %. Recalculation of the hydrogen storage capacity shows that nearly 69 wt % of hydrogen is adsorbed by the carbon phase. This suggests that uniform dispersion of palladium nanoparticles over chemically modified HEG has resulted in about more than three times enhancement in the hydrogen storage capacity of HEG via spillover mechanism. Thus, a nexus of spillover effect and higher surface area of adsorbate has been shown to provide a route to enhance the hydrogen storage capacity, which also meets the theoretically determined optimum thermodynamic conditions for room temperature and moderate pressure ranges.

CONCLUSIONS

Palladium nanoparticles were uniformly dispersed over hydrogen-exfoliated graphene by modified polyol method, which resulted in uniformly dispersed Pd nanoparticles over graphene. The higher surface area of graphene in conjunction with the Pd particles that facilitate hydrogen spillover has been shown to increase the hydrogen storage capacity of HEG by more than three fold. This enhanced storage capacity has been demonstrated at 2 MPa pressure and 25 °C temperature. The isosteric heat of adsorption of hydrogen on Pd/*f*-HEG has been found to be 7−12.5 kJ mol^{-1} and is in agreement with the desirable isosteric heats of adsorption for the potential hydrogen storage media predicted theoretically. The enhancement in the hydrogen storage capacity of Pd/*f*-HEG is attributed to the improved spillover mechanism via functionalization of graphene, which creates good anchoring sites for uniform dispersion of palladium nanoparticles.

ASSOCIATED CONTENT

Supporting Information. This material is available free of charge via the Internet at http://pubs.acs.org.

AUTHOR INFORMATION

Corresponding Author
*Phone: +91-44-22574862, Fax: +91- 44 - 22570509/22574852
Email: ramp@iitm.ac.in.

ACKNOWLEDGMENT

The authors are grateful to Indian Institute of Technology Madras and MNRE for supporting this work.

REFERENCES

(1) Jena, P. *J. Phys. Chem. Lett.* **2011**, *2*, 206–211.
(2) Chambers, A.; Park, C.; Baker, R. T. K.; Rodriguez, N. M. *J. Phys. Chem. B* **1998**, *102*, 4253–4256.
(3) Basca, R.; Laurent, C.; Morishima, R.; Suzuki, H.; Lay, M. L. *J. Phys. Chem. B* **2004**, *108*, 12718–12723.
(4) Ma, L. P.; Wu, Z. S.; Li, J.; Wu, E. D.; Ren, W. C.; Cheng, H. M. *Int. J. Hydrogen Energy* **2009**, *34*, 2329–2332.
(5) Choi, M.; Ryoo., R. *J. Mater. Chem.* **2007**, *17*, 4204–4209.
(6) Jiang, J.; Gao, Q.; Zheng, Z.; Xia, K.; Hu, J. *Int. J. Hydrogen Energy* **2010**, *35*, 210–216.
(7) Orimo, S.; Majer, G.; Fukunaga, T.; Züttel., A.; Schlapbach., L.; Fujii, H. *Appl. Phys. Lett.* **1999**, *75*, 3093–3095.
(8) Geim, A. K.; Novoselov, K. S. *Nat. Mater.* **2007**, *6*, 183–191.
(9) Novoselov, K. S.; Geim, A. K.; Morozov, S. V.; Jiang, D.; Zhang, Y.; Dubonos, S. V.; Grigorieva, I. V.; Firsov, A. A. *Science* **2004**, *306*, 666–669.
(10) Kaniyoor, A.; Jafri, R. I.; Arockiadoss, T.; Ramaprabhu, S. *Nanoscale* **2009**, *1*, 382–386.
(11) Jafri, R. I.; Rajalakshmi, N.; Ramaprabhu, S. *J. Mater. Chem.* **2010**, *20*, 7114–7117.
(12) Panayotov, D. A.; Yates, J. T. *J. Phys. Chem. C* **2007**, *111*, 2959–2964.
(13) Chen, L.; Cooper, A. C.; Pez, G. P.; Cheng, H. *J. Phys. Chem. C* **2007**, *111*, 18995–19000.
(14) Wang, L.; Yang, R. T. *J. Phys. Chem. C* **2009**, *113*, 21883–21888.
(15) Kim, G.; Jhi, S. H.; Lim., S.; Park, N. *Appl. Phys. Lett.* **2009**, *94*, 173102.
(16) Banerjee, S; Pillai, C. G. S; Majumder, C. *J. Chem. Phys.* **2008**, *129*, 174703.
(17) Banerjee, S; Pillai, C. G. S; Majumder, C. *J. Phys. Chem. C* **2009**, *113*, 10574–10579.
(18) Adarsh, K.; Tessy, T. B; Ramaprabhu, S. *J. Mater. Chem.* **2010**, *20*, 8467–8469.
(19) Hummers, W. S.; Offeman, R. E. *J. Am. Chem. Soc.* **1958**, *80*, 1339–1339.
(20) Jeong, H. K.; Lee, Y. P.; Lahaye, R. J. W. E.; Park, M. H.; An, K. H.; Kim, I. J.; Yang, C. W.; Park, C. Y.; Ruoff, R. S.; Lee, Y. H. *J. Am. Chem. Soc.* **2008**, *130*, 1362–1366.
(21) Titelman, G. I.; Gelman, V.; Bron, S.; Khalfin, R. L.; Cohen, Y.; Bianco-Peled, H. *Carbon* **2005**, *43*, 641–649.
(22) Sun, X.; Liu, Z.; Welsher, K.; Robinson, J. T.; Goodwin, A.; Zaric, S.; Dai, H. *Nano Res.* **2008**, *1*, 203–212.

(23) Reich., S.; Thomsen, C. *Phil. Trans. R. Soc. London, Ser. A.* **2004**, *362*, 2271–2288.
(24) Tessy, T. B.; Ramaprabhu, S. *J. Appl. Phys.* **2010**, *108*, 124308.
(25) Jinhua, C.; Mingyong, W.; Bo, L.; Zhen, F.; Kunzai, C.; Yafei, K. *J. Phys. Chem. B* **2006**, *110*, 11775–11779.
(26) Benard, P.; Chahine, R. *Langmuir* **2001**, *17*, 1950–1955.
(27) Yanlk, R. *Vacuum* **1996**, *471*, 205–207.
(28) Srinivas, G.; Zhu, Y.; Piner, R.; Skipper, N.; Ellerby, M.; Ruoff, R. *Carbon* **2010**, *48*, 630–635.
(29) Rubes, M.; Bludsky, O. *Chem. Phys. Chem.* **2009**, *10*, 1868–1873.
(30) Bhatia, S. K.; Myers, A. L. *Langmuir* **2006**, *22*, 1688–1700.
(31) Dipendu, S.; Shuguang, D. *Langmuir* **2009**, *25*, 12550–12560.
(32) Zacharia, R.; Kim, K. Y.; Fazle Kibria, A. K. M.; Nahm, K. S. *Chem. Phys. Lett.* **2005**, *412*, 369–375.
(33) Adams, B. D.; Ostrom, C. K.; Chen, S.; Chen, A. *J. Phys. Chem. C* **2010**, *114*, 19875–19882.
(34) Back, C. K.; Sandí, G.; Prakash, J.; Hranisavljevic, J. *J. Phys. Chem. B* **2006**, *110*, 16225–16231.
(35) Kim, G.; Jhi, S. H. *J. Phys. Chem. C* **2009**, *113*, 20499–20503.
(36) Contescu, I. C.; Brown, C. M.; Liu, Y.; Bhat, V. V.; Gallego, N. C. *J. Phys. Chem. C* **2009**, *113*, 5886–5890.
(37) Bhattacharya, A.; Bhattacharya, S.; Majumder, C.; Das, G. P. *J. Phys. Chem. C* **2010**, *114*, 10297–10301.
(38) Yang, R. T.; Wang, Y. *J. Am. Chem. Soc.* **2009**, *131*, 4224–4226.